Applied Surface Science 412 (2017) 657–667

Contents lists available at ScienceDirect

Applied Surface Science

journal homepage: www.elsevier.com/locate/apsusc

Long term stability of c-Si surface passivation using corona charged SiO_2

Ruy S. Bonilla[a,*], Christian Reichel[b], Martin Hermle[b], Phillip Hamer[a,c], Peter R. Wilshaw[a]

[a] Department of Materials, University of Oxford, Parks Rd, Oxford OX1 3PH, United Kingdom
[b] Fraunhofer Institute for Solar Energy Systems ISE, Heidenhofstr. 2, Freiburg 79110, Germany
[c] School of Photovoltaics and Renewable Energy Engineering, University of New South Wales, Sydney, N.S.W 2052, Australia

ARTICLE INFO

Article history:
Received 20 October 2016
Received in revised form 10 March 2017
Accepted 23 March 2017
Available online 27 March 2017

Keywords:
Surface passivation
Silicon solar cells
Dielectric thin films
Corona discharge

ABSTRACT

Recombination at the semiconductor surface continues to be a major limit to optoelectronic device performance, in particular for solar cells. Passivation films reduce surface recombination by a combination of chemical and electric field effect components. Dielectric films used for this purpose, however, must also accomplish optical functions at the cell surface. In this paper, corona charge is seen as a potential method to enhance the passivation properties of a dielectric film while maintaining its optical characteristics. It is observed that corona charge can produce extreme reductions in surface recombination via field effect, in the best case leading to lifetimes exceeding 5 ms at an injection of 10^{15} cm^{-3}. For a 200 μm n-type 1 Ω cm c-Si wafer, this equates to surface recombination velocities below 0.65 cm/s and J_{0e} values of 0.92 fA/cm^2. The average improvement in passivation after corona charging gave lifetimes of 1–3 ms. This was stabilised for a period of 3 years by chemically treating the films to prevent water absorption. Surface recombination was kept below 7 cm/s, and J_{0e} < 16.28 fA/cm^2 for 3 years, with a decay time constant of 8.7 years. Simulations of back-contacted n-type cells show that front surface recombination represents less than 2% of the total internally generated power in the cell (the loss in power output) when the passivation is kept better than 16 fA/cm^2, and as high as 10% if front recombination is worse than 100 fA/cm^2.

1. Introduction

Crystalline silicon (c-Si) continues to be the leading material for solar cell production. In highly efficient mono c-Si cells, surface recombination of charge carriers is a limiting factor in achieving optimal performance. Reducing surface recombination, also known as surface passivation, is therefore of utmost importance. Furthermore, as cell geometries in which all contacts are on the cell's backside become increasingly popular, front surface passivation becomes even more crucial. The surface in a semiconductor is an abrupt crystal discontinuity. At a bare silicon surface, many atoms may be partially bonded and hence possess dangling bonds that create intermediate band-gap energy levels, also known as surface energy traps or surface states, which promote recombination [1]. In general usage, the term 'surface' refers to a solid–air interface. However, in practical solar cells, bare semiconductor surfaces are not present and recombination actually takes place at interfaces between the semiconductor and other materials, typically dielectrics. As such, the term surface passivation is used here to refer to the mitigation of recombination at such semiconductor–dielectric interfaces. Good surface passivation is commonly achieved via the combined action of a reduction of dangling bonds and a reduction, by use of an electric field, in the concentration of charge carriers at the surface, normally known, respectively, as the chemical effect and the electric field effect [2]. The reduction of minority carrier concentration at the semiconductor–dielectric interface by field effect passivation (FEP) can be achieved by using a field established by charge present in the dielectric film. Dielectric films suited for silicon surface passivation combine a chemical reduction of defect states and a sufficient charge concentration for FEP. Additionally, these films are used as anti-reflection coatings, thus refractive index and absorption become additional variables to be optimised in the film deposition process. If antireflection properties can be decoupled from the passivation efficiency, a very good antireflection film with acceptable chemical passivation can be enhanced for surface passivation by using an additional field effect component, applied after film

* Corresponding author.

http://dx.doi.org/10.1016/j.apsusc.2017.03.204

deposition. We refer to this field effect component as extrinsic FEP. Intrinsic FEP, by contrast, is that achieved by charge generated during film deposition or growth. Optimal surface passivation is hence possible in a dielectric film by exploiting both the chemical and field effect mechanisms, using intrinsic and extrinsic methods.

Recent work on extrinsic field effect passivation has shown it to be a potential method to enhance the passivation properties of a dielectric film while preserving its optical and chemical characteristics [3]. Such extrinsic FEP can be achieved by depositing ions, for example via a corona discharge apparatus, as has previously been reported [4,5]. Previous research has mainly concentrated on the effect of charge on the effective lifetime of minority carriers [6,7], yet very little has been reported about its long term stability and potential as a controlled method for surface passivation. The question remains whether extrinsic charge can be rendered stable such that it becomes of practical relevance for solar cell manufacture. Charged dielectric materials have already been successfully used at industrial level in other fields [8,9]. Such charged dielectric films are also known as *electrets* since they exhibit a quasi-permanent electrical charge. The charge may consist of a net absence or excess of electrons on the dielectric constituent atoms, a net polarisation of the film, or the presence of ionic species within the film matrix [10]. Charge in electrets may occur inherently in some polymers and biological materials. However, electrets are often formed by the external injection of charge using discharges, particle beams, contact electrification, or injection from a deposited metal at high fields [10]. Internal injection of carriers is also possible via heat, or photo injection, but such techniques can physically degrade the dielectric. This work aims to address the possibility to use inorganic oxide electrets as passivation layers for silicon solar cells. For this, the optimal conditions for deposition of charge using corona have been determined and are presented here. The influence of corona charge on a silicon dioxide film is then studied, with emphasis on its effectiveness for silicon surface passivation. The stability of passivation is analysed and approaches are proposed to modify the dynamic behaviour of corona deposited charge on SiO_2. The effect and stability of corona charge in laboratory conditions is reported for periods of over a three years. Lastly, three dimensional simulations of interdigitated (IBC) back contacted cells show that substantial improvement in energy conversion efficiency would be possible if this methodology was adopted.

2. Experimental methodology

2.1. Sample preparation

This study concentrates on n-type monocrystalline silicon with resistivity relevant to solar cell manufacture. 4-in., phosphorous doped, 200 μm thick, planar 1 Ω cm float zone Si wafers were used. Float zone Si is preferred to avoid significant defect related bulk recombination. Wafers were RCA cleaned and HF dipped prior to thermal oxidation in a dry dichloroethylene atmosphere at 1050 °C. 100 nm thick SiO_2 was produced on both sides of the wafers. A forming gas ($5\%H_2/95\%N_2$) anneal (FGA) was then performed in a subset of wafers at 425 °C for 25 min. 3 cm × 3 cm samples were diced from both FGA and none FGA processed wafers. An additional wafer was textured prior to oxidation using an IPA/KOH solution. HMDS chemical treatment was then used to provide a highly hydrophobic coating preventing water from being absorbed into the oxide [7]. Such surface chemical modification of the oxide was applied in two steps. First samples were subjected to a dehydration step in a box furnace at 400 °C for 30 min. They were then immediately moved to a beaker placed on a hot plate with HMDS evaporating at 140–160 °C for 20 min. An improved HMDS coating process was achieved on a second set of samples by placing them in a quartz tube furnace and conducting the dehydration step at 200 °C in an argon atmosphere for 30 min. Without removing the samples from the furnace the temperature was ramped down to 120 °C in ~40 min. Once at 120 °C, the samples were coated with hexamethyldisilazane (HMDS) for 30 min by bubbling argon through an HMDS solution at room temperature before passing the gas over the samples in the furnace. This improved process was only applied to the samples reported in Section 4.3. Ethyl vinyl acetate (EVA, STR Photocap 15455) lamination was conducted in a Spire 230 pin-less laminator at 150 °C for 10 min. This was used to test the stability of the passivation processes to a lamination process typically carried out in solar cell encapsulation.

2.2. Corona discharge

A custom-built corona discharge apparatus was used to deposit charge on the oxide thin films. The corona apparatus consisted of a sharp needle held at a high DC potential (~10–30 kV) and positioned 5–20 cm from the grounded sample. Details of the mechanical design can be found in reference [11]. Here only the corona charging conditions are described. Fig. 1 illustrates the main parameters to consider in a corona discharge rig including the measured current–voltage (*IV*) relation for this set up, including point electrode to sample distances of 8 and 15 cm. Given a point-to-plane distance d_c and a positive corona, a threshold potential V_{Cth} is required before the corona current is produced, Fig. 1b. This was in the order of 7–8 kV for the positive corona. After the corona is started, the current to voltage characteristic follows a linear regime before electric breakdown and sparking at sufficiently high fields. The breakdown regime was not achieved in this rig at 20 kV for a distance d_c of 8 or 15 cm, as illustrated in Fig. 1b. In the case of a negative corona there is no threshold voltage for a corona to start. Corona current is detected at corona potentials as low as 1 kV. Moreover, the *IV* relation for negative corona charge appears more nonlinear than that of positive.

For a set corona distance, the total deposited charge was estimated by integrating the charge per unit time per unit area landing on the sample. For a constant corona current I_c and an effective area for ions to land A_c as illustrated in Fig. 1a, the average concentration of ions at the surface of the specimen is given by:

$$Q_{Cavg} = \frac{1}{A_c}\int_0^{t'} I_c dt = \frac{1}{A_c} I_c t' \quad (1)$$

The effective area A_c has been approximated based on the dimensions of the system here used, considering Warburg's law for a point-to-plane corona system [12,13]. It is noted that for this system the sample cannot be accurately placed in the centre of the plate and this may influence charge uniformity [11,14]. Further details on point-to-plane corona systems can be found on references [11,15,16]. The corona potential and current for extrinsic FEP was selected as follows: FEP in dielectric films has been reported to be produced by a surface concentration of charge in the range 10^{11}–10^{13} q/cm^2 with a typical value of ~10^{12} q/cm^2. When extrinsically adding charge to the dielectric it is desired to produce small incremental improvements in passivation before the charge deposited on the film exceeds the film's breakdown strength, or saturates the improvement in lifetime. For SiO_2 the breakdown electric field strength is 5–10 MV/cm [17]. A field of 5 MV/cm is achieved when a concentration of charge of ~10^{13} q/cm^2 is present at the surface of the dielectric. Eq. (1) shows that a charge concentration of ~3×10^{11} q/cm^2 is deposited on the sample when a 5 s, 1 μA corona discharge is applied to an effective area of 100 cm^2. This allows slow charging before reaching the film's breakdown strength. Following the *IV* characteristics in Fig. 1b, different settings for corona charge

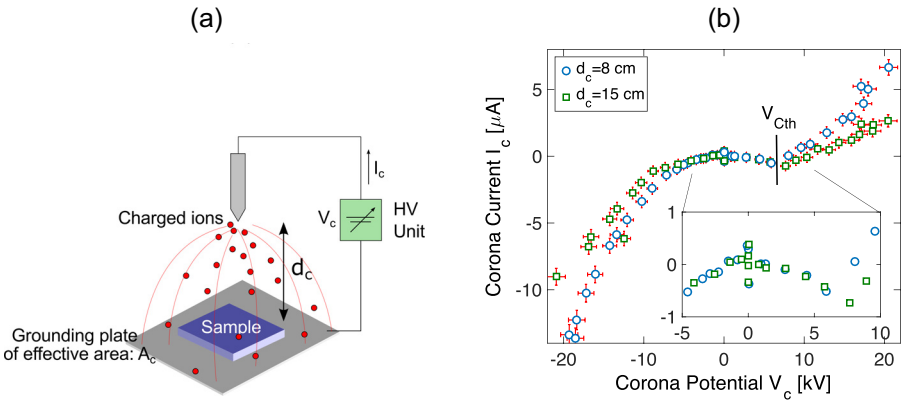

Fig. 1. (a) Schematic of deposition of corona ions including the effective area where ions land, the corona distance, the corona potential and the corona current, (b) current–voltage characteristics of the 8 cm and 15 cm rigs.

were chosen depending on the objective of the experiment. Typical values of corona potential and corona current are $d_c = 15$ cm, $V_c = 15$ kV, $I_c \sim 1$ μA. The smaller the corona distance the worse uniformity of deposited charge as reported in reference [11]. Other factors affecting the corona include the point electrode sharpness, deposition temperature and humidity. Although these were not studied systematically some qualitative remarks can be drawn. Sharper electrodes produce higher local electric fields such that the corona sparks at lower potentials and the corona current increases rapidly. Elevating temperatures also reduces the potential at which the corona sparks and increases the corona current. Humidity has been previously reported to change the level of hydration of the corona ions deposited on the surface yet the *IV* characteristic are minimally changed [18]. $(H_2O)_nH^+$ [19] and $(H_2O)_nH_3O^+$ [20] ion clusters are the main positive charge carriers with a typical n = 4 for ~50% RH, n~8 for high RH, and $n < 4$ for low RH along with formation of $NO^+(H_2O)_n$ and $(NO_2^+)(H_2O)_n$ clusters [19]. In this work standard laboratory conditions (RH~70%, T~20 °C) were used when depositing corona ions.

2.3. Characterisation

Dielectric charge was characterised using Kelvin Probe (KP) measurements as described in [21]. A Scanning Kelvin Probe 3.1 by KP Technology Ltd [10] was used applying Baikie's method [11]. KP measurements were performed immediately after the charge deposition and over an extended period of time to test charge stability. The fixed charge density per unit area, Q_f, at the dielectric surface was estimated as [21]: $Q_f = -\left(\Phi_{ms}/q - V_{Surf}\right)\varepsilon_i/t_i$, where Φ_{ms} is the work function difference between the metal tip and the semiconductor, measured by taking a KP measurement on bare silicon of the same doping concentration, t_i is the thickness of the dielectric coating, q is the electron charge and V_{Surf} is the surface potential measured using KP. This assumes that all charge resides at the surface as demonstrated in [21]. Charge displacement and uniformity was evaluated by mapping kelvin surface potential using a non-feedback *XY* stage actuated by stepper motors. The lateral resolution of the stage was assessed to be ~0.1 mm. Each KP measurement sampled an area ~0.2 mm across.

The effective minority carrier lifetime as a function of the excess minority carrier concentration (Δn) was measured using a Sinton WCT-120 photo-conductance decay (PCD) instrument [22], using both quasi-steady state and transient modes [23,24]. The measurement of carrier recombination in silicon normally results in an effective carrier lifetime τ_{eff} that contains the contributions of the surface and bulk mechanisms. The effective minority carrier lifetime for a silicon specimen as a whole can be expressed as the reciprocal sum of the bulk (radiative and Auger) and surface components, neglecting any bulk defect-mediated recombination:

$$\frac{1}{\tau_{eff}} = \frac{1}{\tau_{Rad}} + \frac{1}{\tau_{Aug}} + \frac{2S_{eff}}{W} \quad (2)$$

where S_{eff} is the effective surface recombination velocity (SRV) and W the thickness of the specimen. Schockley–Read–Hall bulk defect-mediated recombination was neglected since high purity FZ wafers were used, yet it is noted that this may not always be the case [25], and edge effects could be present too [26]. Radiative and Auger recombination were characterised using Richter's parametrisation of intrinsic lifetime [27]. Eq. (2) has been proved accurate to better than 4% when recombination is the same at both surfaces and $\frac{S_{eff}W}{D_p} < \frac{1}{4}$ [28]. The spatial distribution of minority carrier lifetime was characterised using photoluminescence (PL) in a BT Imaging LIS-L1 PL system.

3. Effect of corona charge on SiO_2 passivated c-Si

Deposition of corona charge has been previously reported to reduce surface recombination by means of FEP, thus improving the effective lifetime of minority carriers [29]. This concept, however, has never been studied in detail nor has it been used at industrial scale since corona charge has been seen to decay on a time scale of days to weeks. In this section, we firstly illustrate how much improvement in passivation is possible in silicon relevant to solar applications (~1 Ω cm resistivity). Calculated upper limits to S_{eff} and Emitter saturation current densities J_{0e} are provided in order to compare to the state-of-the-art passivation techniques.

3.1. Extrinsic field effect passivation

Effective lifetime as a function of carrier injection is illustrated in Fig. 2 for oxidised silicon samples deposited with corona charge. Fig. 2a illustrates lifetime measurements for a planar sample, and their corresponding KP measurements of charge concentration. This specimen was subjected to positive corona charge deposition. The effective lifetime was observed to increase from 0.1 to 3.4 milliseconds at $\Delta n = 10^{15}$ cm^{-3}. 3.4 ms lifetime corresponds to an upper limit of surface recombination velocity of 1.6 cm/s when subtracting the Auger and radiative components of the bulk lifetime.

Surface passivation is achieved using two mechanisms: chemical and field effect. The quality of chemical passivation in a dielectric film is determined by the number of interface defect states that remain at the dielectric/silicon interface (D_{it}) after film deposition. Forming gas anneal (FGA) is a standard process to reduce the inter-

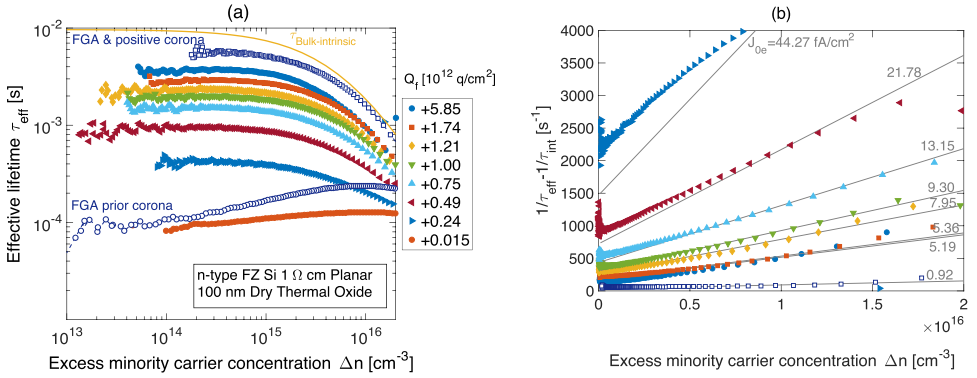

Fig. 2. (a) Lifetime measurements of oxidised planar n-type FZ Silicon when deposited with positive corona charge. Measurements prior and after corona charge deposition on forming gas annealed planar samples are included in the open symbols, (b) corrected inverse lifetime for the corona charged specimen in (a) including the best fitted J_{0e} model of surface recombination.

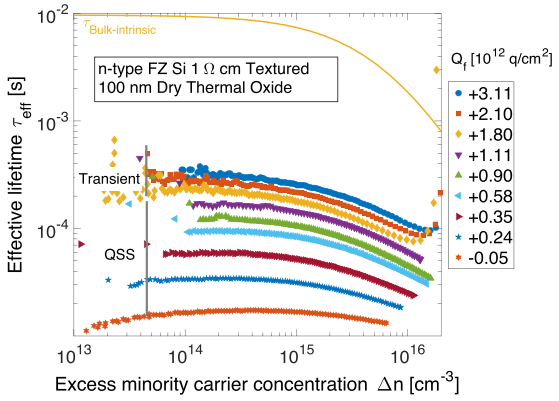

Fig. 3. Lifetime measurements of oxidised planar n-type FZ Silicon when deposited with positive corona charge.

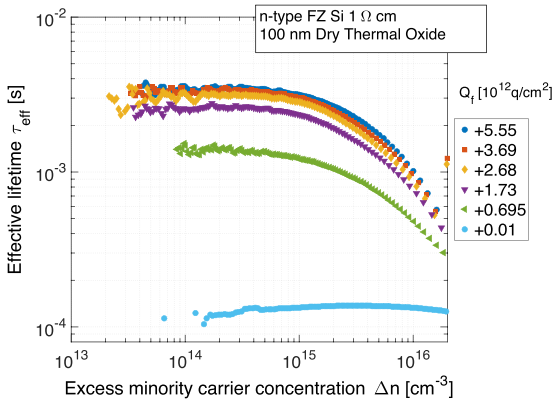

Fig. 4. Lifetime measurements of the oxidised silicon specimen in Fig. 2a after charge removal using isopropyl alcohol and a second deposition of corona charge.

face defect density *after* film deposition extrinsically. A subset of wafers was subjected to a FGA to achieve a better chemical passivation. The improvement in effective lifetime due to extrinsic chemical passivation is illustrated in the open symbols trace at the top of Fig. 2a. The FGA increase in chemical passivation resulted in a lifetime improvement up to 5.2 ms at $\Delta n = 10^{15}$ cm^{-3}. This equates to an upper limit of SRV of 0.65 cm/s.

J_{0e} values for these passivated specimens can be estimated in a number of ways. Approximation (5) in [30] is commonly used leading to $J_{0e} = 4$ fA/cm^2 for bare oxides or $J_{0e} = 1.45$ fA/cm^2 for FGA oxides. Here, a more accurate estimation of J_{0e} was achieved using an adaptation of Kane and Swanson's method [31]: a function $f(J_{0e}) = 1/\tau_{eff} - 1/\tau_{int} = 2 \times J_{0e}\left(N_{dop} + \Delta n\right) / \left(qWn_i^2\right)$ was fitted to the $1/\tau_{eff} - 1/\tau_{int}$ experimental data using the least squares method in the $\Delta n = [4\text{–}16] \times 10^{15}$ cm^{-3} range with J_{0e} as the only fitting parameter. The intrinsic lifetime τ_{int} was calculated using Richter's parametrisation [27]. The experimental data, fitted $f(J_{0e})$ functions, and extracted J_{0e} values are illustrated in Fig. 2b. For bare oxides a $J_{0e} = 5.19$ fA/cm^2 was calculated while FGA oxides produced a $J_{0e} = 0.92$ fA/cm^2.

The front surface of solar cells is commonly textured to enhance light trapping. Field effect surface passivation of a double-sided textured specimen has also been tested here. A 3 cm × 3 cm sample underwent the same oxidation step to produce a 100 nm film. It was then corona charged until additional charge no longer improved effective lifetime. This is illustrated in Fig. 3 including the inferred charge concentrations from KP measurements. In this textured Si sample the effective lifetime was observed to increase from 0.015 to 0.25 ms at $\Delta p = 10^{15}$ cm^{-3}. This is an increase of ~10 fold with a charge concentration of $\sim 3 \times 10^{12}$ q/cm^2. This compares well with the lifetime increase achieved on planar surfaces, yet the overall recombination (lifetime) is substantially higher (lower). Several early reports on the interface characteristics of Si/SiO$_2$ have shown that <111> surfaces have 5–10 times higher interface state densities [32–34]. This, in addition to the ~70% increase in surface area in a pyramidal textured surface, account for such lower lifetime achieved in the textured specimen in Fig. 3, compared to a planar one in Fig. 2a.

3.2. *Influence of surface corona charge in the SiO$_2$/c-Si interface*

Excessive deposition of corona charge has been observed to damage permanently the passivation properties of the oxide-silicon interface. Fig. 4 shows the effective lifetime of the same sample in Fig. 2a after it has been rinsed in isopropyl alcohol to eliminate all surface charge, and is corona charged a second time. On the second charging cycle, a similar concentration of charge was deposited, but the effective lifetime reached a maximum value of 3 ms at a minority injection level of 10^{15} cm^{-3}, compared to 3.4 ms in the first cycle. Comparison of Fig. 2a with Fig. 4 shows that when the surface charge exceeds ~5×10^{12} q/cm^2 the chemical passivation properties of the film deteriorate. The mechanisms of passivation damage or deterioration due to corona discharge were studied by combining PCD lifetime measurements, PL imaging, and KP surface potential measurements.

Two specimens were corona charged using a tip-sample distance $d_c = 5$ cm to reduce uniformity below 50% over a ~20 cm^2 area, and study regions of high and low charge concentration at the same time. Lifetime and spatial resolved photoluminescence were recorded as the charge was increased in 5–10 s intervals, Fig. 5.

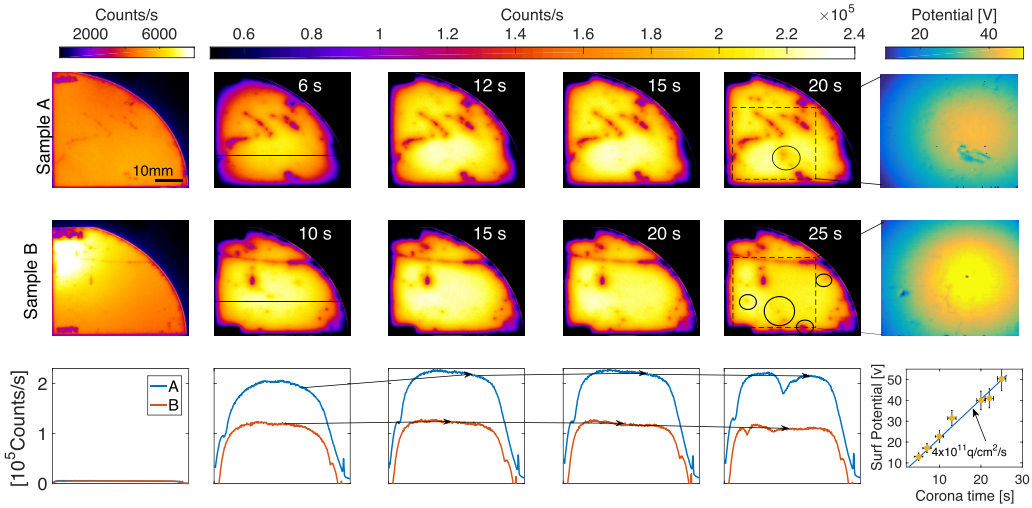

Fig. 5. Photoluminescence of two oxidised FZ n-Si specimens as a function of charging time in a corona rig with $d_c = 5$ cm and $V_c = 10$ kV. PL bias photon flux 9.46×10^{16} cm^{-2} s^{-1}. Black circles in 5th column indicate damaged regions. Bottom row shows the PL intensity of a cross section at the location indicated by the white lines in the second column. Arrows indicate progression of the PL intensity as charge increases. Right column shows Kelvin probe surface potential maps at the end of the charging experiment.

After 15–20 s of corona charging, equivalent to a surface potential of ~30 V and a surface charge concentration of $\sim 6 \times 10^{12}$ q/cm^2, it was observed that an overall reduction of PL intensity, thus effective lifetime, took place in large areas (>10 mm^2) of both samples. This decrease in lifetime is similar to that observed in the second cycle of corona charged applied to the sample in Fig. 4. Additionally, several mm-size regions of low lifetime seem to get formed as corona charge is increased beyond a saturation point, here observed to occur after ~15 s of corona charge. These damaged regions are evident on both samples in Fig. 5 and have been indicated by the black circles in the last PL image of the charging sequence. Kelvin probe surface potential maps were performed at the end of this charging cycle for both samples, last row in Fig. 5. The surface potential showed no correlation to the damaged (low PL intensity) regions marked in the black circles. A charge deposition rate plot was included in Fig. 5 for this corona rig; $d_c = 5$ cm and $V_c = 10$ kV. The spatial PL images in Fig. 5 also show the strong reduction in carrier lifetime at the edge of the specimens as a result of unpassivated cleaved edges and sample handling.

A cross-section along the x-axis was included at the bottom of Fig. 5 for the PL intensity 15 mm from the bottom of both samples – the position shown by the horizontal white lines in the second PL images. These were averaged over 5 pixels to account for misalignment recording the PL intensity. These cross-sections clearly show the non-uniform increase in sample lifetime as corona is deposited on the surface of the oxide. The arrows point out the change in PL intensity of a region in both samples where PL is seen to decrease after ~15 s of corona charge, termed here as weak damage regions. Additionally, the cross section in the last charging step shows dips in the PL, strong damage regions, after excessive charge is deposited. These two types of damage can arise from different mechanisms. Firstly, electrical breakdown of the dielectric can lead to high conductivity channels in the oxide where oxide-silicon bonds break thus deteriorating the passivation qualities of the interface. Given the uniformity observed in the KP potential maps, such channels are of micron scale and do not reduce the charge concentration substantially. Such charge produces a field lower than the breakdown strength of SiO_2 typically reported [17], yet the work of Nakamura [35], Schuegraf [36,37] and Verweij [38] showed that other conduction mechanisms are activated at lower field strengths, and these may produce damage of the Si/SiO_2 interface. The regions circled in the last charging step of Fig. 5 could present such a damage mechanism. Secondly, Black and McIntosh

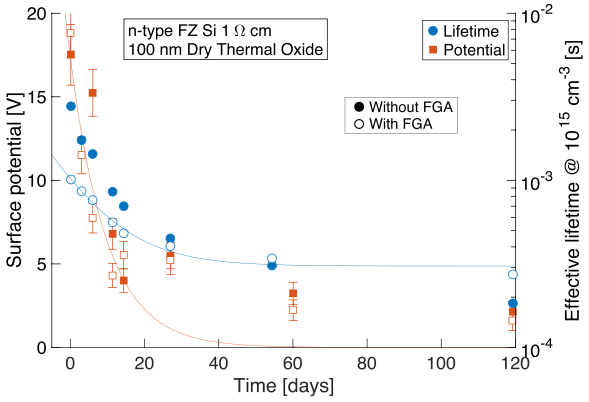

Fig. 6. Kelvin probe (KP) surface potential and effective lifetime @ $\Delta n = 10^{15}$ cm^{-3} of c-Si oxidised specimens after corona charge deposition. Solid lines show the best fitted single exponential decay model for lifetime and surface potential in samples without FGA.

[39] proposed that some deterioration of the chemical passivation at the Si/SiO_2 interface could be caused by electron photoemission from the silicon which may then promote hydrogen release from the interface. For this work it can only be concluded that chemical de-passivation takes place by one or both of these models.

4. Stability of corona charge in SiO_2 passivated Si

4.1. Corona charge leakage

It has been shown that corona discharge can produce very effective extrinsic passivation of silicon surfaces. Before this passivation technique can be used at a practical level, it must be shown to be stable for a lifetime comparable to that of a solar cell (~25–30 years). The stability of corona charge was evaluated by recording the KP surface potential and effective lifetime for a period of time after charge deposition. For this experiment, 3 cm × 3 cm samples from FZ wafers with the same thermal 100 nm oxide were deposited with corona charge to optimal passivation levels as described in Section 2. KP and lifetime measurements thereafter are illustrated in Fig. 6. Specimens that did and did not undergo FGA were investigated. Regardless of the forming gas anneal, the surface potential in all samples decayed to pre-corona levels within 60 to 120 days. A sin-

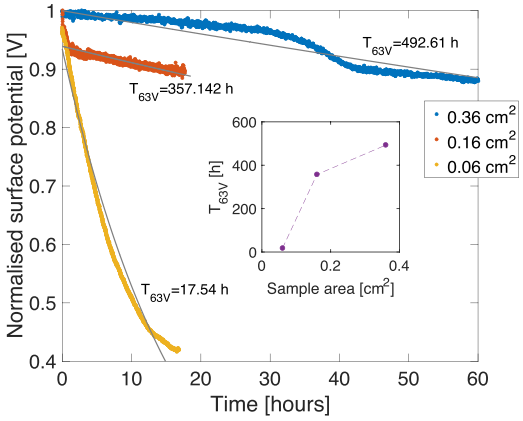

Fig. 7. Kelvin probe (KP) surface potential and effective lifetime for HMDS treated and corona charged 100 nm oxide specimens. (a) No FGA treatment. (b) FGA treatment. Solid lines show the exponential decay function fitted to the experimental data.

gle exponential decay term was fitted to the lifetime decay curve as $\tau = (\tau_c - \tau_0)e^{-t/T_\tau} + \tau_0$ with corona charged lifetime τ_c and decay time constant T_τ as fitting parameters, and pre-corona lifetime τ_0 defined by the first measurement prior to any corona deposition in the sample. Similarly, for surface potential a decay function $V_{surf} = V_0 e^{-t/T_V}$ was fitted. Stability of passivation and dielectric charge is here quantified using T_τ and T_V parameters. For these specimens $T_\tau = 9.4 \pm 2$ days and $T_V = 12.5 \pm 2$ days. The fitted curves are included for the samples without a forming gas anneal in Fig. 6. The description of KP measurements in Section 2.3 showed that a decrease in KP surface potential can be caused either by a decrease in charge concentration, or a decrease in the distance of the charge to the dielectric/silicon interface. In the latter case, the net concentration of charge would remain unchanged and FEP would be maintained. Here it is evident that the decay in surface potential relates well to the decay in surface passivation quality. Additionally, at any point during the test period, other samples were rinsed with isopropanol (IPA) and the charge was immediately removed, thus eliminating the FEP component. This confirmed that charge associated with the oxide remained at the surface, even many days after deposition.

The decay mechanism of corona charge in silicon dioxide has previously been reported to be due to the loss of charge by lateral surface conduction on the film [5]. Studies by Olthuis and Bergveld [5,40] demonstrated that SiO_2 maintained corona charge poorly due to its large lateral surface conductivity rather than its bulk conductivity. They concluded that conduction was due to silanol (SiOH) groups created at or near the surface of the oxide by chemisorption of water. Specifically, conduction took place via mobile protons in SiOH groups, or via hydrogen hopping in water molecules physisorbed to the SiOH groups. Additionally, they showed that these phenomena could happen through the first 40 nm of SiO_2 thin films. To corroborate these observations, three specimens with surface areas as low as 0.06 cm^2 were corona charged with similar concentrations to those reported in Section 3. The decay in surface potential in all specimens was measured over a short period of time by leaving the sample in the KP instrument for 20–60 h to avoid any errors arising from change in the measurement place. Fig. 7 illustrates the surface potential measured as a function of time for each sample. Here, it is evident that smaller samples, in which the surface path to the edge is smaller, present a higher decay rate thus supporting the surface conduction mechanism as the main leakage mechanism.

It is also noted that no report has been found on the compensation of corona charge due to dust, air molecules or stray ions present in the environment attaching to the film and screening charge. Results in Section 4.2 corroborate that no external compensation mechanism is observed. Despite the presence of SiOH groups, Olthuis and other authors [5,9,41,42] have reported that SiO_2 could store corona charge when the surface conductivity is reduced using a chemical surface modification. This modification is shown next.

4.2. Chemical surface modification of SiO_2

Olthuis et al. [5,40] demonstrated that the surface of SiO_2 films could be chemically modified to prevent water absorption, and hence surface conductivity. They proposed that a hydrophilic to hydrophobic conversion of the oxide surface was possible using a hexamethyldisilasane (HMDS) protective coating. HMDS effectively substitutes SiOH groups with polar trimethyl silyl groups that prevent proton conduction or water physisorbtion [43,44]. A set of 3 cm × 3 cm oxidised c-Si samples were treated with HMDS prior to corona charge deposition. After charging to a surface potential of ~13 V ($Q_f \sim 2.7 \times 10^{12}$ q/cm^2), the specimen lifetime and surface potential were measured over a period of 3 years. These measurements are illustrated in Fig. 8. All samples were stored in plastic bags in laboratory conditions without temperature, humidity or atmospheric control. It is important to note that optical losses due to the intermediate HMDS film have not been characterised here but assumed to be minimal since this process forms a monolayer film.

The stability of passivation produced by corona charge is here evaluated over a long measurement period. It was observed that a fast decay component occurred during the first 50–100 days reducing lifetime by 10–15%. After this initial period, a single exponential decay function (Section 4.1) was fitted and a time constant of effective lifetime $T_\tau \sim 900 \pm 300$ days was calculated for samples that did not undergo FGA prior to HMDS and corona charging, Fig. 8a. The surface potential in this specimen was seen to decay slower with a $T_V \sim 8000 \pm 1000$ days, thus showing that a thin SiO_2 film is an effective electret material. Although charge does not notably decrease, lifetime is seen to slowly decay over the whole period. The effective lifetime initially increases to 2 ms after corona charging, producing a SRV upper limit of 3.7 cm/s at an injection level of 10^{15} cm^{-3}, $J_{0e} < 7.8$ fA/cm^2. After 1200 days passivation quality has decayed and the effective lifetime is 0.9 ms. SRV_{UL} is ~ 9.7 cm/s, $J_{0e} < 22.1$ fA/cm^2.

HMDS surface treatment was also applied to a specimen that underwent a FGA, gure 8.b. This specimen was corona charged to optimal passivation, $V_s \sim 20$ V ($Q_f \sim 4.2 \times 10^{12}$ q/cm^2), stored under laboratory conditions, and measured over a period of 1000 days. The effective lifetime before corona charge deposition is seen to increase from ~0.2 ms to ~2 ms. This increase in surface passivation is not as effective as that previously illustrated in Section 3.1 since in the 3 cm × 3 cm sample here used lifetime is strongly limited by edge recombination [26]. Once again, a fast ($T_{63} \sim 20$ days) decay of lifetime was observed in the first 50 days, yet the HMDS chemical treatment stabilised the passivation quality thereafter, evidenced by time constants of $T_\tau \sim 3200 \pm 500$ days and $T_V \sim 30k \pm 1k$ days. Surface charge was seen virtually constant over the measurement period while a small decrease in passivation took place. After 1000 days the passivation quality has decayed and the effective lifetime is 1.2 ms and SRV is ~7 cm/s, $J_{0e} = 16.28$ fA/cm^2.

4.3. Lateral charge migration in HMDS treated oxides

Lateral charge migration after the improved HMDS chemical treatment (Section 2.1) was assessed by mapping the surface potential of a specimen using Kelvin Probe measurements straight after corona deposition, Fig. 9a, and two years later, Fig. 9b.

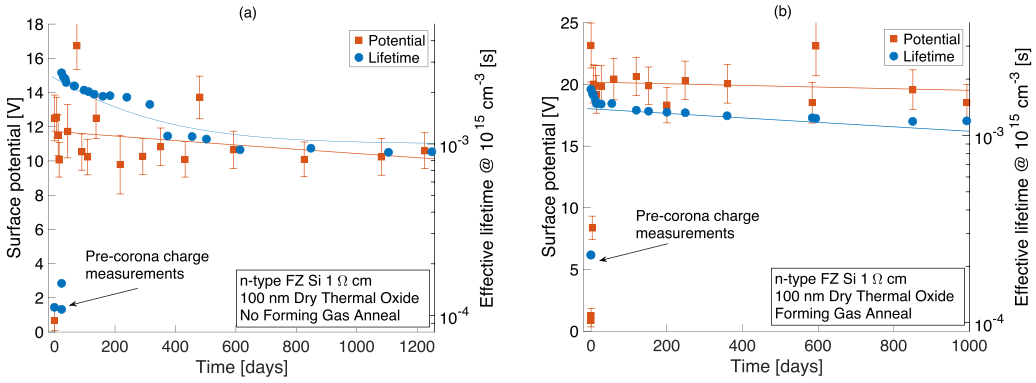

Fig. 8. Kelvin probe (KP) surface potential and effective lifetime for HMDS treated and corona charged 100 nm oxide specimens. (a) No FGA treatment. (b) FGA treatment. Solid lines show the exponential decay function fitted to the experimental data.

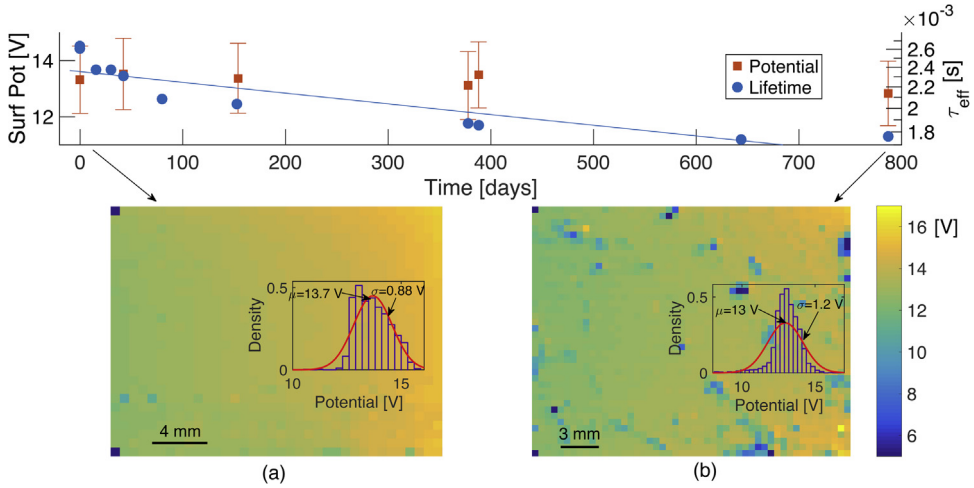

Fig. 9. The time and spatial variation of the charge induced surface potential and effective lifetime over 2 years. Kelvin Probe surface potential maps of a 100 nm oxidised FZ specimen, HMDS treated, right after corona charge deposition (a), and after two years in laboratory conditions (b).

Here, it was confirmed that the uniformity of corona charge deposition using $d_c = 15$ cm was very good ($V_{surf} = 13.7\,V \pm 0.88\,V$, $Q = 2.8 \pm 0.08 \times 10^{12}$ q/cm^2). Charge mapping of the same specimen two years later revealed the presence of many small regions with substantially lower surface potential than the neighbouring regions. The average surface potential after two years, however, was only reduced by 0.7 V. This indicates a decay time constant for KP surface potential of $T_V \sim 14.8k \pm 1k$ days. A decay time constant of effective lifetime of $T_\tau \sim 2000 \pm 500$ days was calculated. The fitted curve is included in Fig. 9. Lateral charge migration after two years was not observed to occur, at least on the scale of 1 mm given by the resolution of the KP instrument. This mapping experiment demonstrates that lateral migration can be eliminated when HMDS removes the surface conduction on the oxide, such that corona charge will not neutralise thanks to water induced conduction across the surface. Despite this, small, reduced charge regions can arise either from sample manipulation or, more likely, the previously mentioned channels in the dielectric where small amounts of conduction might take place.

4.4. Effect of EVA lamination

While it is essential that the extrinsic field enhanced passivation is stable over operational time periods, to be industrially relevant, the passivation must also survive a typical solar cell lamination process. In order to investigate the stability of the passivation through the lamination process, an HMDS treated and corona passivated wafer was laminated with EVA. Recombination in the samples was characterised using transient photo-conductance decay and PL imaging with a BTi R1 tool [45]. The photoluminescence images were post processed using PLPro software [46] to perform point square deconvolution using the method of Teal and Juhl [47]. In order to ensure that the laminate did not interfere with photoconductance measurements the Sinton WCT-120 instrument was zeroed with a layer of cured laminate prior to characterisation of the laminated wafer.

The results in Fig. 10 clearly indicate that there has been an increase in recombination at the surface as a result of the lamination process. The minority carrier lifetime measured at $\Delta n = 10^{15}$ cm^{-3} decreased from 4.6 ms to 3.4 ms. While this represents a significant decrease in effectiveness there is evidently still significant field effect passivation. Furthermore, it is notable that the field effect passivation is stable after lamination with the lifetime showing no observable degradation over the subsequent 6 months.

Given the thermal stability of oxide passivation on silicon the increase in surface recombination is ascribed to a decrease in charge at the oxide surface rather than an increase in interface trap density. Charge could be lost to the EVA layer or through lateral transport to regions of high leakage current such as the wafer edges. The PL images in Fig. 10 indicate that the increase in surface recombination is nearly uniform with no observable change in gradients towards the edges or regions of low charge density. This supports the explanation that ions are leaking into the EVA at the elevated temperature.

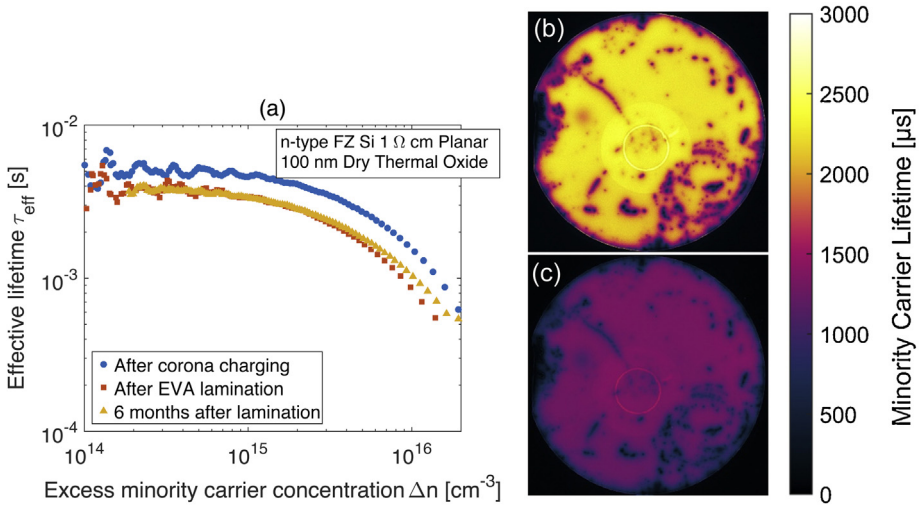

Fig. 10. (a) Injection level dependent lifetime measured using transient photo-conductance after corona charging (orange squares), after EVA lamination (yellow triangles) and 6 months after lamination (purple stars), (b) calibrated photoluminescence lifetime image taken before EVA lamination at an average injection level of $\Delta n = 6.2 \times 10^{15}$ cm^{-3}, (c) calibrated photoluminescence lifetime image taken after EVA lamination at an average injection level of $\Delta n = 3.6 \times 10^{15}$ cm^{-3}. It should be noted that both images were taken with the same illumination intensity and that the bright circles visible on the images are an optical effect from the induction coil. (For interpretation of the references to color in this figure legend, the reader is referred to the web version of the article.)

5. Extrinsic field effect front surface passivation in IBC cells

The performance of interdigitated back contact (IBC) cells is strongly reliant on the diffusion of minority carriers from the place where they are generated, near the front surface, to the emitter and BSF where they get collected. The two main loss mechanisms in this process are the recombination of carriers in the bulk, and at the surface of the cell. The former is normally dealt with by having a clean silicon feedstock and clean processing steps in the manufacture. The latter, on the other hand, is addressed by producing a light n-type diffusion which provides field effect passivation to the cell's front surface. This light diffusion is commonly termed a front surface field (FSF). When present, the field effect component of passivation is mainly provided by this FSF and thus the dielectric fixed charge is of lesser importance. However, if the FEP can be effectively and *stably* provided by the charge in the dielectric, the FSF would no longer be needed thus reducing both the processing complexity and thermal budget, and also Auger recombination losses. The possible replacement of a FSF by using stable dielectric charge is studied here by simulating an IBC cell using Quokka 2.2.4 [48].

The cell reported by Reichel et al. in [49] was used as a model. It was adapted to evaluate the significance of charge associated with the dielectric film and the front surface field produced. Front surface recombination was parameterised using the dark recombination current density J_{0e} parameter, which in turn was varied to model different recombination rates taking place at the front of the cell. The parameters for the modelled IBC cell were taken to approximate as close as possible those obtained for a large emitter coverage, structure A, in [49]. These are listed in Table 1. Fig. 11a illustrates the scheme of the unit cell simulated including the dimensions of the back diffusions and back contacts. Fig. 11b illustrates the simulated IBC cell performance when front surface passivation is varied. J_{0e} values ranging from 1 to 1000 fA/cm^2 were simulated in this IBC cell to cover and extend those experimentally found in Section 3. This simulations show that the cell performance depends strongly on passivation of the front surface, particularly when the quality of the front surface passivation is poor ($J_{0e} > 100$ fA/cm^2). A loss in efficiency of over 6% absolute is observed as front surface recombination worsens to $J_{0e} \sim 1000$ fA/cm^2. Open circuit voltage and short circuit current also deteriorate yet the collection efficiency, and thus J_{sc}, is more strongly affected since near-surface photo-generated carriers are lost to surface recombination. When the passivation quality is improved from $J_{0e} \sim 100$ fA/cm^2 to $J_{0e} < 10$ fA/cm^2, an increase of over 1.5% in absolute efficiency is seen, with an efficiency as high as 24% for this IBC model cell. Similarly, open circuit voltage and short circuit current density as high as 708 mV and 40.8 mA/cm^2 are possible. The inset in Fig. 11b illustrates a simulation of the J_{0e} parameter performed in PC1D as suggested by Cabanas-Holmen and Basore [50]. The effective SRVs were calculated using approximation (5) in [30] for $\Delta n = 10^{15}$ cm^{-3} and are displayed in the right hand *y*-axis in the inset of Fig. 11b. This simulation comprises a lightly doped *pn* junction in the dark, with and without a highly doped front surface layer equivalent to the n+ front surface field (FSF) in an IBC cell – i.e. $R_s = 150$ Ω/sq. The J_{0e} parameter was obtained by calculating the dark saturation current density of this diode for a varying concentration of charge at the surface of the *n-type* semiconductor in the *pn* junction. It is clear that the presence of a FSF reduces significantly the dependence of surface recombination, thus J_{0e}, on FEP from dielectric charge. However, in the absence of a FSF, an extremely well passivated surface can be produced purely by field effect ($J_{0e} \sim 2$ fA/cm^2) exceeding the performance of a FSF since Auger recombination losses are avoided in

Table 1
IBC cell parameters for simulation.

Name	Value
Cell thickness	180 µm
Base resistivity (n-type)	1 Ω cm
SRH bulk lifetime ($\tau_n = \tau_p$)	2.5 ms
Emitter diffusion sheet resistance	90 Ω/□
Base diffusion sheet resistance	50 Ω/□
Front surface field sheet resistance	150 Ω/□
Un-diffused rear J_0, passivated	2 fA/cm^2
Emitter diffusion J_0, passivated	19 fA/cm^2
Emitter diffusion J_0, contacted	417 fA/cm^2
Base diffusion J_0, passivated	215 fA/cm^2
Base diffusion J_0, contacted	583 fA/cm^2
Emitter contact resistance	5×10^{-5} Ω cm^2
Base contact resistance	1×10^{-5} Ω cm^2
External series resistance	0.1 Ω cm^2
External shunt resistance	10^5 Ω cm^2
Intrinsic carrier concentration	9.65×10^9 cm^{-3}

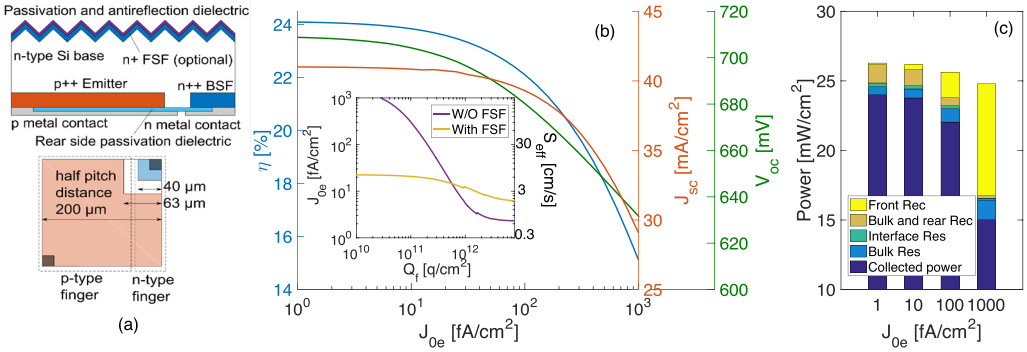

Fig. 11. (a) Schematic of IBC solar cell simulated in Quokka including dimensions of the back fields and contacts dimensions, (b) simulated performance of the IBC cell as a function of front emitter saturation current, inset: Simulated dependence of J_{0e} as a function of front surface charge in the dielectric for a *n* silicon surface with and without a front surface field, (c) energy loss analysis of the simulated IBC cell including the power collected and power lost from bulk and interface resistive losses, and from rear, bulk and front recombination losses.

the absence of a FSF. In this work, experimental values of J_{0e} as low as 0.92 fA/cm^2 are reported, Section 3.1, thus showing that the FEP associated with a charged dielectric film can deliver better performance than that of a FSF. It is noted that these simulations both in Quokka and PC1D do not account for the extra recombination that takes place in a textured surface as that present in the front side of a solar cell. From the results in Section 3.1 it is evident that even with the best passivation quality the recombination is about one order of magnitude higher in the textured surface.

Finally, Fig. 11c illustrates the energy loss analysis in this simulated cell. When the front surface is extremely well passivated, its effect is negligible and the internally generated power is as high as 26.28 mW/cm^2, as expected from the larger V_{oc} and V_{mpp} obtained when the quasi-Fermi levels are farther apart. As the front surface passivation is reduced, substantial losses arise and less internal power is available. Typical experimental values of J_{0e} are in the 20–100 fA/cm^2 range [49,51,52], yet it is clear that values well below 10 fA/cm^2 are desirable for optimal cell performance.

6. Discussion

The use of corona charge on oxidised FZ-Si has been shown to produce a strong reduction of surface recombination provided by extrinsic FEP. When corona charge is deposited on top of thermally grown oxides, SRV < 2 cm/s, J_{0e} < 7 fA/cm^2 are readily achieved at a minority carrier injection of 10^{15} cm^{-3}. When oxides are additionally submitted to a forming gas anneal surface recombination parameters reduce to SRV < 0.6 cm/s, J_{0e} < 3 fA/cm^2 upon corona charge deposition. To the authors' knowledge, this is among the lowest surface recombination velocity achieved on ~1 Ω cm n-type crystalline silicon passivated with a thermal oxide. This level of passivation compares or outperforms several state-of-the-art processes including the 'alneal' process reported by Kerr and Cuevas [53], the oxide/PECVD nitride layers used by Larionova [54], the remote PECVD nitride used by Richter [27] and fast ALD AlO_x reported by Werner [55]. This comparison is outlined in Fig. 12. It is evident that the controlled and uniform FEP methods used here (and in previous publications by the same authors) are as effective and, in some cases, better than state-of-the-art and expensive technologies. Additionally, extrinsic FEP allows more flexibility in the combined optimisation of the optical properties, and the chemical and field effect passivation properties of dielectric films. If implemented at solar cell level, silicon dioxide films with enhanced chemical and FEP as reported in this work could be used in combination of optically optimal films, such as silicon nitride or titanium oxide. This makes extrinsic passivation a potential technology to further reduce recombination losses in high efficiency silicon solar cells. Furthermore, the versatility, low cost and now improved stability of extrinsic FEP makes it an extremely promising passivation approach to be used at the industrial scale.

When applied to a textured surface, extrinsic FEP produces a proportional reduction in surface recombination velocity yet effective lifetimes achieved are substantially lower (one order of magnitude) than for planar surfaces. This is not surprising since, in textured Si, the passivated surface is a <111> face of the pyramidal structure, rather than the <100> face of a planar one, and <111> faces have approximately 5–10 times higher state densities [32–34] at the Si/SiO_2 interface, and a ~70% increase in surface area. Surface recombination has rarely been studied on textured surfaces, yet these are the ones used in practical Si solar cells. From these results, however, it is noted that although textured <111> surfaces present less chemical passivation, the effectiveness of FEP in increasing lifetime is comparable to that achieved on a <100> surface. It is also noted that the calculation of effective SRV and the J_{0e} parameter used for planar surfaces does not directly apply to a textured one [59], thus values of these surface recombination parameters have not been reported for the textured silicon used here.

This work has also shown a step towards solving the stability issue when using extrinsic corona charge passivation. Surface conduction due to silanol groups and water absorption was identified as the primary source of charge leakage. This leakage was largely eliminated by HMDS treating the thermally grown SiO_2 films at low temperatures, 100–200 °C. In treated oxide films, retention of charge was reported for periods exceeding 3 years, the longest reported on an inorganic electret film. The quality of surface passivation, however, decreased with a decay time constant of ~1000 days. When the dielectric film had undergone a FGA, corona charge was equally stable while effective lifetime decayed at a slower rate, with time constant of ~3000 days. Overall, these methods showed that a substantial improvement in the stability of surface passivation can be achieved, thus showing a real potential of extrinsic FEP to be used in industrial manufacture of silicon solar cells.

In this work it was also found that some deterioration of the passivation takes place over long periods of time despite observing that the charge concentration averaged throughout the sample surface is very stable. The charge stability was tested both using single-point measurements, and larger area maps of surface potential. When using single-point measurements, no decay could be observed over 3.5 years given the accuracy of the KP instrument. Using KP potential mapping, on the other hand, a number of small ~1–3 mm^2 regions with partially lost charge where detected after 1.5 years in laboratory conditions, yet no lateral migration could be evidenced within the lateral resolution of the technique. This

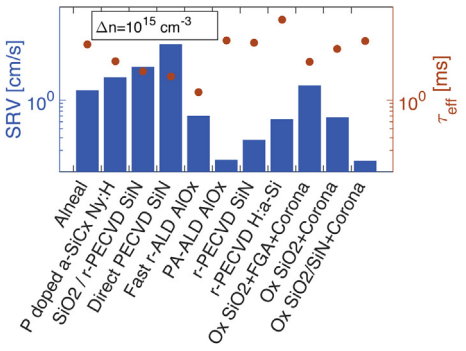

Passivation	Material	Ref
Alneal	n-FZ, 1.5 Ωcm	[53]
P doped a-SiCxNy:H	n-FZ, 1 Ωcm	[56]
SiO2/ r-PECVD SiN	n-Cz, 2.5 Ωcm	[54]
Direct PECVD SiN	n-FZ, 1.5 Ωcm	[57]
Fast r-ALD AlOx	n-FZ, 1 Ωcm	[55]
PA-ALD AlOx	n-FZ, 1 Ωcm	[27]
r-PECVD SiN	n-FZ, 1 Ωcm	[27]
r-PECVD H:a-Si	n-FZ, 3 Ωcm	[58]
Ox SiO2+FGA+Corona	n-FZ, 1 Ωcm	-
Ox SiO2+Corona	n-FZ, 1 Ωcm	-
Ox SiO2/SiN+Corona	n-FZ, 1 Ωcm	[11]

Fig. 12. Comparison of record passivation quality obtained using state-of-the-art techniques and the passivation achieved using the techniques proposed in this work ('Ox' suffix), [56–58].

indicates that HMDS is effectively eliminating lateral conduction mechanisms in the oxide, yet there seems to be a number small 'bad' spots on the oxide. These small, low surface potential regions suggest that a component of bulk conduction in the oxide is present at those regions, presumably caused by small break down channels. This leads to leakage of the corona charge through the oxide, and it is more commonly observed at high surface potential regions. It is also possible that this may be due to sample manipulation and storage, or imperfections in the wet oxide growth process as revealed by PL imaging in Section 3.2. Despite this leakage component, the average surface potential for the measured specimen only reduced by 0.7 V ($\sim 5 \times 10^{10}$ q/cm^2). Given the lateral resolution of the surface potential mapping, it is not possible to infer if the overall reduction in surface passivation is only due to a loss of charge. The results here suggest that the reduction in overall surface passivation is mainly due to a loss in the chemical quality of the interface, and a small loss in field effect passivation provided by the corona charge. When corona charging oxide films it was also observed that an oversaturation of charge could lead to a chemical loss in passivation quality, both in small millimetre sized regions, and large areas of the sample. This would appear to be a chemical de-passivation mechanism related to the high electric field at the interfaces. Two models have been suggested for this mechanism. Firstly, the creation of micro-breakdown channels product of weakening of the dielectric [17]. Secondly, the hydrogen release from the Si/SiO_2 interface due to highly energetic electrons photo-emitted from the Si [39]. The exact nature of the de-passivation mechanism was not studied in this work; thus it is only proposed here that one or both of these mechanisms could be responsible for the loss in passivation.

Despite the improved stability of corona FEP in these oxide films, the small decay in passivation observed could hinder the energy output of solar cells in the long term. To evaluate this, the direct effect of front surface passivation on the performance of an IBC cell has been assessed using simulations on Quokka. The device parameters reported by Reichel in [49] were chosen to simulate a model cell and evaluate the effect of recombination at the front surface. It was shown that all cell parameters are sensitive to front recombination, especially when the passivation is poor. Efficiency and J_{sc} were more susceptible to changes in front surface passivation. The energy loss analysis conducted showed that when the front surface J_{0e} was kept below 20 fA/cm^2, as would be the case in the specimen in Fig. 8 after 3.5 years, the percentage of power loss from front surface recombination was below ~25% of the total losses, and only ~2.3% of the total internally generated power. If, on the other hand, front surface passivation degrades to $J_{0e} > 100$ fA/cm^2, the front recombination contributes to >50% of the total power losses, and >8% of the internally generated power.

When data in Figs. 2 and 3 is placed in the context of these simulations, it is possible to see that a decay in J_{0e} from 7.2 to 23 fA/cm^2, similar to that observed experimentally after 3.5 years, is equivalent to a reduction of 0.33% absolute efficiency, $\Delta V_{oc} > 7$ mV, and $\Delta J_{sc} > 0.23$ mA/cm^2. With a decay time constant $T_{63\tau} \sim 3200$ days (best obtained in the present work) the experimental effective lifetime of the specimens in this work would extrapolate to about 200 μs in 30 years, leading to $J_{0e} \sim 100$ fA/cm^2. Efficiency would thus reduce by ~2% absolute, $\Delta V_{oc} > 25$ mV, and $\Delta J_{sc} > 1.6$ mA/cm^2. This shows that despite the great effectiveness of corona field effect surface passivation, the small decay observed over the 3 years of these measurements still seems greater than that required for a commercial solar cell intended to last for 25–30 years. In addition, HMDS is an organosilicon compound and no report of its long term stability in harsh environmental conditions has been published to date. HMDS is thus unlikely to be a practical solution for silicon solar cells that must endure ultraviolet radiation, humidity, and thermal bonding to polymers for cell encapsulation. It is hence required to have further improvements in the stabilisation of the passivation.

7. Conclusions

In the present work it has been demonstrated that FEP can be applied extrinsically to thermally grown silicon dioxide to improve its passivation quality, producing lifetimes as high as 5 ms at an injection of 10^{15} cm^{-3}, which equate to surface recombination velocities below 0.65 cm/s, on n-type 1 Ωcm c-Si, equivalent to J_{0e} values of 2.88 fA/cm^2. Both planar and textured silicon surfaces showed a decrease in surface recombination of 2–10 times when charged using corona discharge. These results show that very large improvements in the passivation properties of films can be achieved by modifying their charge density. Average improvements of 1–3 ms were routinely obtained and stabilised for periods of at least three years. Chemical processing of the oxide was observed to be a requirement for long term stability. SRVs below 7 cm/s were demonstrated by the end of the measurement period indicating a decay time constant of the passivation of 3200 days. The chemical treatment applied represents a potential method to produce controlled and stable field effect passivation for solar cells, yet the stability needs to be extended to the lifespan of a practical solar cell because simulated solar cells showed an extrapolated decrease in passivation to $J_{0e} \sim 100$ fA/cm^2 after 30 years.

Acknowledgments

RS Bonilla is the recipient of an EPSRC (UK) Postdoctoral Research Fellowship, EP/M022196/1. P Hamer and PR Wilshaw acknowledge the support from EPSRC grant EP/M024911/1. All

authors are thankful to John Murphy and Nicholas Grant for help with photo-luminescence measurements using the system under EPSRC First Grant (EP/J01768X/2) at the University of Warwick, and to Brett Hallam for insightful discussions. Data published in this article can be downloaded from http://ora.ox.ac.uk.

References

[1] S.M.S. Sze, N. Kwok Kwok, K.K. Ng, Physics of Semiconductor Devices, third ed., John Wiley and Sons, Inc., Hoboken, New Jersey, 2007.
[2] A.G. Aberle, Prog. Photovolt. 8 (2000) 473–487.
[3] R.S. Bonilla, P.G. Hamer, P.R. Wilshaw, EUPVSEC, Munich, Germany, 2016, pp. 707–710.
[4] J. Schmidt, A.G. Aberle, Prog. Photovolt. 6 (1998) 259–263.
[5] W. Olthuis, P. Bergveld, IEEE Trans. Electr. Insul. 27 (1992) 691–697.
[6] T.C. Kho, S.C. Baker-Finch, K.R. McIntosh, J. Appl. Phys. 109 (2011) 6.
[7] S.W. Glunz, D. Biro, S. Rein, W. Warta, J. Appl. Phys. 86 (1999) 683–691.
[8] H. Amjadi, C. Thielemann, IEEE Trans. Dielectr. Electr. Insul. 3 (1996) 494–498.
[9] R. Kressmann, G.M.M. Sessler, P. Gunther, P. Günther, IEEE Trans. Dielectr. Electr. Insul. 3 (1996) 607–623.
[10] G.M. Sessler, Electrets, second ed., Springer, Berlin, Germany, 1987.
[11] R.S. Bonilla, F. Woodcock, P.R. Wilshaw, J. Appl. Phys. 116 (2014) 54102.
[12] B.L. Henson, J. Appl. Phys. 52 (1981) 3921.
[13] E. Warburg, Handbuch Der Physik, 14, Springer, Berlin, 1927.
[14] F. Woodcock, Passivation of Semiconductor Surfaces for High-Efficiency Solar Cells, Oxford, 2014.
[15] R.B. Comizzoli, J. Electrochem. Soc. 134 (1987) 424.
[16] M. Goldman, A. Goldman, R.S. Sigmond, A.G.M. Goldman, R.S. Sigmond, M. Goldman, A. Goldman, R.S. Sigmond, Pure Appl. Chem. 57 (1985) 1353–1362.
[17] C.M. Osburn, D.W. Ormond, J. Electrochem. Soc. 119 (1972) 591.
[18] I. Faulkner, Corona Enhanced Oxidation of Materials, University of Oxford, 2013.
[19] M.M. Shahin, J. Chem. Phys. 45 (1966) 2600.
[20] J.D. Skalny, J. Orszagh, S. Matejcik, N.J. Mason, J.A. Rees, Y. Aranda-Gonzalvo, T.D. Whitmore, Int. J. Mass Spectrom. 277 (2008) 210–214.
[21] R.S. Bonilla, N. Jennison, D. Clayton-Warwick, K.A. Collett, L. Rands, P.R. Wilshaw, Energy Procedia 92 (2016) 326–335.
[22] www.sintoninstruments.com, 2017.
[23] R.A. Sinton, A. Cuevas, M. Stuckings, Photovolt. Spec. Conf. 1996. Conf. Rec. Twenty Fifth IEEE, 1996, pp. 457–460.
[24] R.A. Sinton, A. Cuevas, Appl. Phys. Lett. 69 (1996) 2510.
[25] N.E. Grant, F.E. Rougieux, D. Macdonald, Solid State Phenom. 242 (2015) 120–125.
[26] R.S. Bonilla, G. Martins, P.R. Wilshaw, Solid State Phenom. 242 (2016) 73–79.
[27] A. Richter, S.W. Glunz, F. Werner, J. Schmidt, A. Cuevas, Phys. Rev. B 86 (2012) 165202.
[28] A.B. Sproul, J. Appl. Phys. 76 (1994) 2851.
[29] S.W. Glunz, D. Biro, S. Rein, W. Warta, J. Appl. Phys. 86 (1999) 683.
[30] H. Mäckel, K. Varner, Prog. Photovolt. Res. Appl. 21 (2013) 850–866.
[31] D.E. Kane, R.M. Swanson, Proc 18th IEEE Photovolt. Spec. Conf., 1985, pp. 578–583.
[32] M.H. White, J.R. Cricchi, IEEE Trans. Electron. Dev. 19 (1972) 1280–1288.
[33] M.L. Reed, J.D. Plummer, J. Appl. Phys. 63 (1988) 5776.
[34] E.H. Nicollian, J.R. Brews, MOS (Metal Oxide Semiconductor) – Physics and Technology, Wiley, New York, 1982.
[35] K. Nakamura, T. Takahashi, T. Hikichi, I. Takata, Proc. Int. Symp. Power Semicond. Devices IC's ISPSD '95, Inst. Electr. Eng., Japan, 1995, pp. 374–379.
[36] K.F. Schuegraf, IEEE Trans. Electron. Dev. 41 (1994) 1227–1232.
[37] K.F. Schuegraf, C. Hu, J. Appl. Phys. 76 (1994) 3695.
[38] J.F. Verweij, J.H. Klootwijk, Microelectron. J. 27 (1996) 611–622.
[39] L.E. Black, K.R. McIntosh, IEEE Trans. Electron. Dev. 57 (2010) 1996–2004.
[40] J.A. Voorthuyzen, W. Olthuis, P. Bergveld, A.J. Sprenkels, IEEE Trans. Electr. Insul. (1989).
[41] H. Nung-Pyo, H. Jin-Woong, Proc. 2004 IEEE Int. Conf. Solid Dielectr, ICSD 2004, IEEE, 2004, pp. 170–173.
[42] P. Gunther, IEEE Trans. Electr. Insul. 26 (1991) 42–48.
[43] V. Leonov, P. Fiorini, C. Van Hoof, IEEE Trans. Dielectr. Electr. Insul. 13 (2006) 1049–1056.
[44] H. Amjadi, IEEE Trans. Dielectr. Electr. Insul. 6 (1999) 852–857.
[45] T. Trupke, R.A. Bardos, M.C. Schubert, W. Warta, Appl. Phys. Lett. 89 (2006) 44107.
[46] D.N.R. Payne, M.K. Juhl, M.E. Pollard, A. Teal, D.M. Bagnall, IEEE 43rd Photovolt. Spec. Conf., 2016.
[47] A. Teal, M. Juhl, IEEE 42nd Photovolt. Spec. Conf., IEEE, 2015, pp. 1–5.
[48] A. Fell, IEEE Trans. Electron. Dev. 60 (2013) 733–738.
[49] C. Reichel, F. Granek, M. Hermle, S.W. Glunz, Prog. Photovolt. Res. Appl. 21 (2012).
[50] P.A. Basore, K. Cabanas-Holmen, 27th Eur. Photovolt. Sol. Energy Conf. Exhib, 2012, pp. 1462–1464.
[51] F. Granek, C. Reichel, Sol. Energy Mater. Sol. Cells 94 (2010) 1734–1740.
[52] C. Reichel, M. Bivour, F. Granek, M. Hermle, S.W. Glunz, Phys. Status Solidi 208 (2011) 2871–2883.
[53] M.J. Kerr, A. Cuevas, Semicond. Sci. Technol. 17 (2002) 35–38.
[54] Y. Larionova, V. Mertens, N.-P. Harder, R. Brendel, Appl. Phys. Lett. 96 (2010) 32105.
[55] F. Werner, B. Veith, V. Tiba, P. Poodt, F. Roozeboom, R. Brendel, J. Schmidt, Appl. Phys. Lett. 97 (2010) 162103.
[56] R. Ferre, A. Orpella, D. Munoz, I. Martín, F. Recart, C. Voz, J. Puigdollers, P.R. i Cabarrocas, R. Alcubilla, Prog. Photovolt. Res. Appl. 16 (2008) 123–127.
[57] A. Rohatgi, P. Doshi, J. Moschner, T. Lauinger, A.G. Aberle, D.S. Ruby, IEEE Trans. Electron. Dev. 47 (2000) 987–993.
[58] J.-W.A. Schuttauf, K.H.M. van der Werf, I.M. Kielen, W.G.J.H.M. van Sark, J.K. Rath, R.E.I. Schropp, Appl. Phys. Lett. 99 (2011).
[59] K. Xiong, S. Lu, D. Jiang, J. Dong, H. Yang, Appl. Phys. Lett. 96 (2010) 193107.